15th IFK
Proc. of the 15th International Fluid Power Conference <Symposium/Conference>
<DOI>

Investigation of Fatigue Crack Growth under high Pressure Gradients with a Fluid-Structure-Interaction Model

Blatter, Fabian[1*]; Boden, Lukas[2]; Schmitz, Katharina[2]; Geimer, Marcus[1]

1. *Institute of Mobile Machines, Karlsruhe Institute of Technology, Germany*
2. *Institute for Fluid Power Drives and Systems, RWTH Aachen University, Germany*

* fabian.blatter@kit.edu

Abstract.

Hydraulic components in mobile machinery are increasingly exposed to dynamic high-pressure gradients, which can accelerate fatigue crack growth and affect component reliability. This study investigates fluid-induced fatigue crack propagation by implementing a newly developed test specimen within an existing fluid–structure interaction (FSI) simulation framework. The specimen was designed to enable reproducible crack initiation, measurable crack propagation, and efficient manufacturability for experimental validation. FSI simulations were conducted across multiple crack lengths and pressure loading configurations to examine the influence of pressure drop and build-up rates. The results indicate that fluid effects, such as hydrostatic pressure and fluid-induced crack closure, modify the effective stress intensity factor (effective SIF) and the corresponding crack growth rates. While the observed trends are generally consistent with Paris' law, the influence of pressure gradients appears limited within the investigated range. Overall, the study highlights existing gaps in understanding fluid-induced crack propagation in hydraulic components and underscores the need for further experimental and numerical investigations, particularly given contradictory findings in previous work.

Keywords. Fluid-structure interaction, fatigue crack propagation, fluid-induced crack closure, pressure gradients

1. INTRODUCTION

Hydraulic systems are frequently exposed to highly dynamic load changes during operation that result in significant and constant changes of pressure. High pressure gradients can occur in different components of a hydraulic system such as axial piston pumps or throttle and orifice geometries of valves. Pressure gradients of up to 1.000 kbar/s have been reported for some of these components [1]. Previous studies have shown that drop rates of pressure in particular have an influence on the propagation rate of fatigue cracks [2, 3]. Under such

conditions, fatigue strength becomes a more decisive criterion. Although design strategies exist that successfully increase the service life of critical regions, they cannot fully eliminate fatigue-related failures. As a result, material fatigue remains a fundamental challenge.

The challenge intensifies in the context of mobile hydraulic applications and increasing power densities, where lightweight components offer clear advantages. However, the reduced and targeted material use required for lighter constructions also increases the likelihood of crack failure. Therefore, a strong need exists to better understand and predict crack growth mechanisms in hydraulic components.

The present work investigates fluid-induced fatigue crack growth using a FSI approach. A new test specimen is developed and implemented within an existing FSI simulation framework originally proposed by Michiels [4]. The paper focuses on the design of this test specimen and on the presentation of simulation results obtained with the updated test specimen. The simulation framework has so far been tested with only one specimen and has shown limitations. These limitations motivate further investigations, particularly with regard to the influence of pressure gradients on fatigue crack growth. The simulation results presented in this paper serve as reference data for future comparisons, including pressure distributions within the crack, calculated SIFs, and resulting crack propagation rates. The updated specimen will be used for the development and validation of a new FSI approach that addresses the limitations of the current framework. The overarching goal of this research is to enable a reliable estimation of crack growth rates of fluid-induced fatigue cracks, which could be used to define inspection intervals for hydraulic components or to replace critical parts prior to failure.

2. Effects on Crack Propagation of Fluid-filled Cracks

This research focuses on fatigue crack propagation in hydraulic components under cyclic loading. Specifically, it investigates fluid-filled cracks, where crack growth is driven by pressurized fluid both inside and outside the crack. In fracture mechanics, several parameters are essential to describe crack behaviour under cyclic loading. The most fundamental loading case mode I (opening mode) is shown in Figure 2.1, where the load acts perpendicular to the x-z-plane and drives the crack faces apart [5].

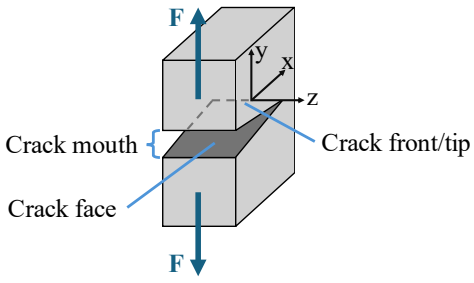

Figure 2.1. Description of the crack mode I (opening mode) and components of the crack

The governing parameter for characterizing the stress field at the crack tip is the stress intensity factor (SIF) K. It is described by the far-field applied stress σ, the current crack length a in x-direction and the geometric correction factor f as [5]:

$$K = \sigma\sqrt{\pi a} \cdot f \qquad (2.1)$$

The R-ratio defines the ratio of minimum to maximum stress σ_{min} and σ_{max} in a load cycle [6]:

$$R = \frac{\sigma_{min}}{\sigma_{max}} \qquad (2.2)$$

The SIF range ΔK is the difference between the minimum and maximum SIF [6]:

$$\Delta K = K_{max} - K_{min} \qquad (2.3)$$

Paris' law from 1963 shows that a decreasing SIF range ΔK reduces the crack propagation. It expresses the relationship between the crack propagation rate da/dN (N is the number of applied cycles) and the SIF range ΔK together with the constants C_p and m_p that depend on the material, temperature, environmental medium and load as [7]:

$$\frac{da}{dN} = C_p \cdot \Delta K^{m_p} \qquad (2.4)$$

Typically, no load is applied to the crack faces [5]. If hydrostatic fluid pressure acts on the crack faces it increases the crack propagation rate [3]. The penetration of fluid also influences the contact behaviour of the crack surfaces. When a pressure drop occurs rapidly in a fluid-filled crack, the fluid cannot completely escape and remains trapped inside the crack. The fluid remaining in the crack indirectly connects the crack faces and prevents a complete return to the original state. When the load is increased again, the crack remains closed to a certain load level. As a result, the crack is not open during the entire loading cycle. Crack closure was first discovered by Elber [8]. Figure 2.2 shows the curve of the SIF over time with and without crack closure effect. In the following, the SIFs are denoted with the subscript I, since the loading discussed in this paper is predominantly mode I.

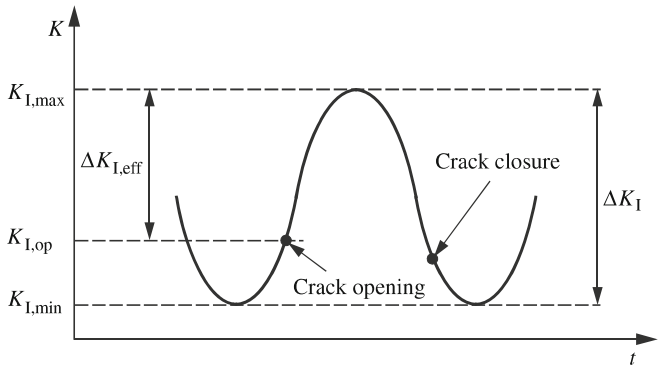

Figure 2.2. Comparison of the SIF with and without crack closure effect [9]

With crack closure effects the effective SIF range $\Delta K_{I,eff}$ is reduced. According to Paris' law it can extend a component's lifetime compared to a crack without entrapped fluid [9, 10]. The classical computation of the SIF ΔK_I doesn't cover shielding effects like crack closure

[11]. Therefore, the effective SIF range $\Delta K_{I,eff}$ covering crack closure is calculated with the maximum applied SIF $K_{I,max}$ and the crack opening SIF $K_{I,op}$ [9, 10]:

$$\Delta K_{I,eff} = K_{I,max} - K_{I,op} \qquad (2.5)$$

Other known crack closure phenomena are plasticity induced, roughness induced, and oxide induced crack closure. Plasticity-induced closure originates from residual deformation in the crack wake, roughness-induced closure from mismatch of the fracture surfaces, and oxide-induced closure from the buildup of corrosion products [5].

Investigations of fluid-induced crack closure are primarily found in related research fields, for example on railway wheel–rail systems and submerged fatigue specimens. For submerged specimens, it has been demonstrated that fluid-filled fatigue cracks exhibit a reduced crack propagation rate compared to air-filled cracks. This is due to fluid-induced crack closure and the reduced effective SIF ΔK_{eff}. [12]

Similar mechanisms have been identified in railway tracks, where fatigue cracks propagate mainly due to entrapped fluid. Under rolling contact, surface cracks open due to traction forces, allowing fluid to penetrate the crack. As the wheel passes and forces the crack mouth to close, the trapped fluid becomes pressurized, generating tensile and shear stresses on the crack faces that accelerate crack growth in the direction of wheel motion. [13, 14, 15] In the absence of fluid, such crack growth is largely suppressed [15].

Numerical and experimental investigations of pressurized cracks have shown partially contradictory results. In [4], simulations of fully fluid-filled cracks indicated that neither the pressure build-up rate nor the pressure drop rate significantly affect the stress amplitude at the crack tip and therefore the crack propagation rate. In contrast, corresponding experiments showed a significant influence of the pressure drop rate on the crack propagation rate.

Despite these studies, the mechanisms behind fluid penetration into fatigue cracks in hydraulic components are not fully understood. There is a lack of systematic investigation into how externally pressurized fluids penetrate and interact with fatigue cracks under cyclic loading. Furthermore, how the interaction of the fluid with the mechanical structure affects the effective SIF of fatigue cracks in hydraulic components has not been fully quantified. Addressing these questions constitutes a critical research gap, especially for the reliable lifetime prediction of hydraulically loaded components under cyclic loading.

3. INTRODUCTION TO FSI APPROACH OF MICHIELS

The interaction between solids and fluids is a multi-physics problem, which is addressed in this study through a two-way fluid–structure coupling. The FSI framework is proposed by Michiels [4] and is summarized in this chapter with a focus on its most relevant characteristics. For a detailed description, the reader is referred to the original publication. The FSI approach avoids fully fluid and structural simulations (e.g. through the finite element method) and instead employs reduced-order models for both the structural and fluid domain. Input parameters for the FSI model include the applied load, weight functions, and flow factors. Weight functions correlate the load to the structural deformation, while flow factors account for roughness effects in narrow crack flows. Both were determined prior in pre-processing steps. The simulation is conducted for a fixed crack length. The resulting outputs of the coupled FSI are the pressure field and fluid flow inside the crack and its crack

opening displacement (COD). The crack is discretized into N stripes with a constant length Δx, shown in Figure 3.1. This model is referred to as strip model and uses the same discretization for the fluid inside the crack.

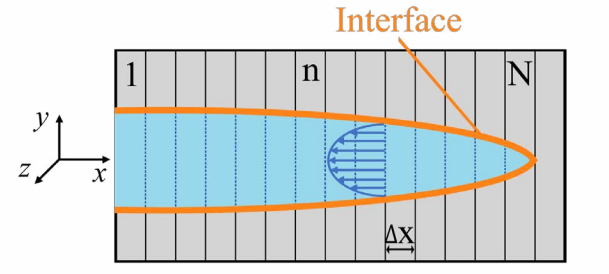

Figure 3.1. Discretization of the crack and the fluid into N stripes. The structural domain is shown in grey, the fluid domain in blue and the interface between both in orange.

Fluid pressure acting on the crack faces is transferred to the structural domain, while the resulting structural displacements are transferred back into the fluid domain, shown in the following Figure 3.2.

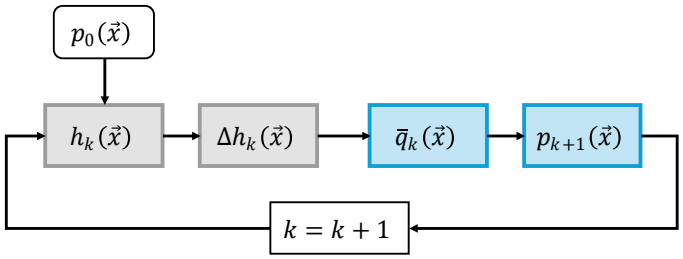

Figure 3.2. Iteration through the two-way coupled FSI with the structural domain in grey and the fluid domain in blue during a timestep k.

At the first timestep k = 0, the initial pressure p_0 is given as 0 bar and transferred to the mechanical domain. The crack height h is calculated with the given arbitrary pressure p and the weight functions, in the following given in matrix notation as W, while ξ describes the centre of a stripe.

$$h(\vec{x} = \vec{\xi}) = \mathbf{W}p(\vec{x}) \qquad (3.1)$$

The used weight functions depend only on the geometry including the crack and are independent from the applied load. They are calculated for the examined specimen with discrete crack lengths via finite element method in a pre-processing step. The detailed calculation procedure of the weight functions can also be found in [4]. Assuming linear elastic material behaviour, the total deformation is obtained by superposition of the deformations induced by individual load contributions. The pressure force acting from the fluid on the crack surface is decomposed into N+1 subparts. One associated with the displacement caused by external forces, like a pressure chamber, and N corresponding to the individual crack sections called stripes.

The resulting structural displacement Δh calculated from equation 3.1 is transferred to the fluid domain. The fluid domain describes the fluid flow inside the crack as a planar flow, neglecting the crack width, and is modelled using an adapted thin-film flow formulation, which is appropriate due to the small crack opening relative to its length. The governing equations are derived from the Navier–Stokes equations under laminar flow assumptions and discretized along the crack using the same spatial resolution as the structural strip model. In addition, the fluid flow is assumed to be fully developed, which is consistent with the neglect of fluid inertia effects. To account for the influence of surface roughness on flow resistance, flow factors are introduced. They represent the reduction in flow capacity caused by rough crack surfaces. The use of flow factors $\theta \in [0,1]$ enables the model to capture roughness-induced flow restriction without explicitly resolving surface topography. They compare the average pressure flow through rough gaps relative to that through smooth gaps. The average Reynolds equation using flow factors was introduced by Patir and Cheng in 1978 [16, 17]. The averaged volume flow per unit length $\bar{q}$ along the crack in x-direction is given by

$$\bar{q} = -\theta \frac{h^3}{12\eta} \frac{\partial p}{\partial x} \qquad (3.2)$$

where h denotes the crack opening and η the dynamic viscosity. For a perfectly smooth surface θ equals 1. The pressure p of the following time step k = k + 1 is calculated by the following equation with the density ρ, reference density ρ_0 and the bulk modulus K:

$$\frac{\partial p}{\partial t} = -\left(\frac{\partial(\rho \bar{q})}{\partial x} + \rho \frac{\partial h}{\partial t}\right) \frac{K}{\rho_0 h} \qquad (3.3)$$

4. TEST SPECIMEN GEOMETRY

A test specimen geometry was proposed by Michiels in [4], which is shown in Figure 4.1. It contains an internal pressure chamber with a notch. Under pressurization, mechanical deformation and stress are induced. Due to the increased stress concentration at the notch root, a crack initiates from this location and subsequently propagates. Since the crack originates from the interior pressure chamber, it remains in contact with the pressurized fluid, that can flow into and out of the crack. The fracture process is predominantly Mode I.

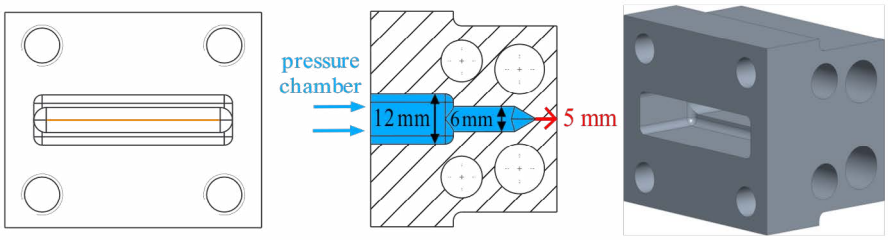

Figure 4.1. Proposed test specimen in [4]. Test specimen contains four threaded holes, a pressure chamber (blue), a notch (orange) and four relief holes. The ligament of the uncracked specimen with a length of 5 mm is shown in red.

According to [4], the experimental configuration enables a stable crack growth regime without causing catastrophic rupture of the structure, allowing the influence of fluid-induced crack closure and fluid flow within the crack to be investigated. Furthermore, it provides a basis for assessing the transferability between planar two-dimensional simulations and three-dimensional test specimens. However, several limitations are associated with this specimen design for experiments on a hydraulic test rig:

- The specimen geometry is complex (threads, geometry of pressure chamber, relief holes) and therefore requires considerable time to manufacture. For future investigations a broader validation campaign is planned with a larger number of specimens to investigate several load configurations (see chapter 4).
- Manufacturing constraints, as a sharp notch cannot be produced with conventional machining like milling. A residual radius remains and varies due to tool wear, resulting in geometric inconsistencies.
- Crack initiation can occur at any location along the notch shown in Figure 4.1, which reduces reproducibility. Also, several cracks can be initiated along the notch during testing.
- The remaining ligament is short, allowing a maximum crack extension of only 5 mm. A longer ligament provides more opportunities to monitor relevant crack growth effects and allows observations over a larger crack length.
- The internal volume is comparatively large. Since the objective is not to measure compression-induced volumetric flow, a minimal dead volume is required.
- Crack breakthrough was observed only after averaged 812k load cycles, representing an excessively high cycle count.

Therefore, a new test specimen is proposed. The following additional requirements are defined for its geometry:

- Less complex test specimen geometry to ensure efficient and reproducible production as well as economical manufacturability.
- Sufficient remaining ligament to allow measurable crack growth and data acquisition over a range of crack lengths.
- Reproducible crack initiation at a defined location within the specimen with only one crack developing per test specimen.
- Rapid crack initiation to minimize the number of load cycles required in total.
- Consistent crack length through minimal geometric variation between specimens in the region from the notch to the opposite side.
- Minimal plastic deformation, as excessive plastic strain may alter the material properties within the plastic zone and distort the fracture behaviour.
- Reduced internal volume to minimize the influence of compression-induced flow.
- Surfaces parallel and perpendicular to crack growth for sensor installation (strain gauge, temperature sensor, acoustic emission sensor).

According to those defined by Michiels and the additional requirements, a new specimen was developed (see Figure 4.2). A parameter study was conducted for the final geometric dimensions, varying the geometric properties of the specimen to achieve a favourable stress distribution for an assumed pressure of 400 bar.

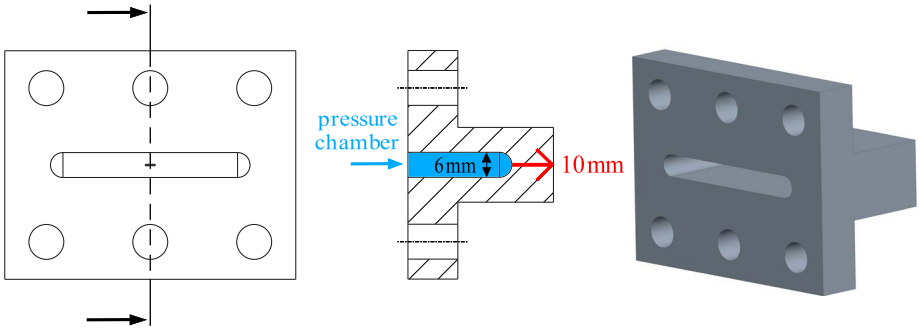

Figure 4.2. Updated test specimen according to the defined requirements. It contains a pressure chamber (blue) and six through holes for connecting the specimen to an adapter of the test stand. The ligament of the uncracked specimen with a length of 10 mm is shown in red.

In the revised specimen design, through holes were implemented instead of threaded holes, eliminating one manufacturing step. The threaded holes were relocated to the adapter, and due to the more slender geometry no relief holes were required. The pressure chamber was designed with a simplified geometry and its dead volume was reduced from 16221.3 mm^3 to 6816.35 mm^3, corresponding to a reduction of 58 %. Furthermore, the ligament thickness was increased from 5 to 10 mm in order to extend the achievable crack length. To ensure consistency across all manufactured test bodies, a more precise tolerance was introduced, resulting in a ligament length with a total deviation of 0.25 mm.

A considerable amount of lifetime is spent in crack initiation [9, 18, 19]. To shorten this phase and define a starting point for crack growth as defined above, micro-notches are introduced in the form of five micro-drilled holes. Cracks usually propagate from discontinuities in geometry like holes, notches or shoulders, where stress concentrations occur. The use of micro-drilled holes for this purpose is a common practice in fracture mechanics testing, as shown in [20, 21]. In the section view of the test specimen in Figure 4.3 the micro-notches are implemented at the center of the inner cavity. This study also focuses on crack propagation rather than initiation, as effects such as crack closure mainly occur during the propagation phase.

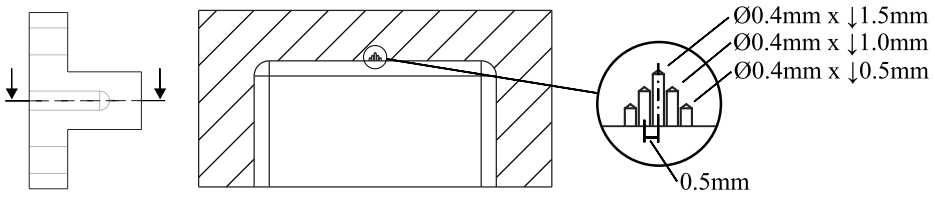

Figure 4.3. Sectional view of the test specimen showing the five micro-drilled holes inserted as micro-notches for a defined crack initiation.

To evaluate the stability of crack growth, a fatigue crack simulation was carried out using the SMART simulation tool within the FEM software Ansys [22]. The initial crack geometry was derived by the outer contour of the five micro-notches. For the crack propagation

simulation Paris' law and the material parameters $C_p = 1.25 \cdot 10^{-9}$ and m_p = 3.38 were used [9]. A maximum pressure of 400 bar and an R-ratio of 0.1 were applied. Also, no FSI inside the crack was considered for this step. Figure 4.4 shows the simulated crack front geometries for different crack lengths.

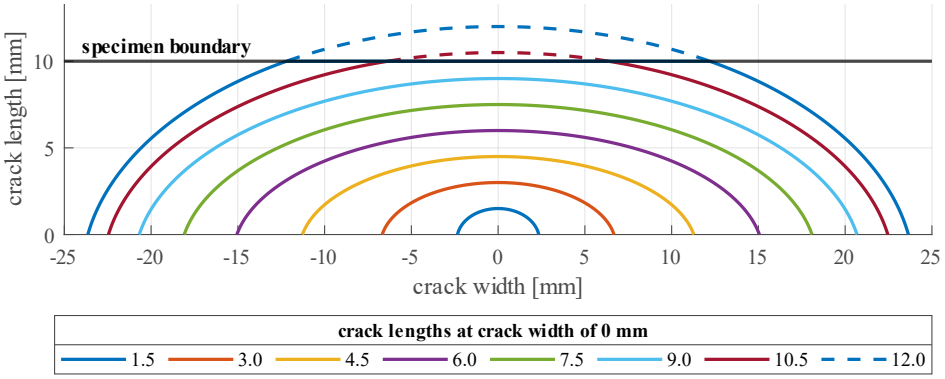

Figure 4.4. Approximated crack front geometries for several crack lengths

The calculated ΔK_I values for crack lengths between 1.5 and 10 mm are presented in Figure 4.5, starting at 1.5 mm due to the micro-notches. The values of ΔK_I remain above the threshold for fatigue crack growth of S235 for R=0.1, $\Delta K_{I,th}$ = 10.2 MPa√m [9]. For structural steels in general, ΔK_{IC}-values between 50 and 150 MPa√m are common [23]. Consequently, the results indicate that stable fatigue crack growth is expected under the investigated loading conditions. The final steep increase in ΔK_I is caused by the reduction in remaining ligament length.

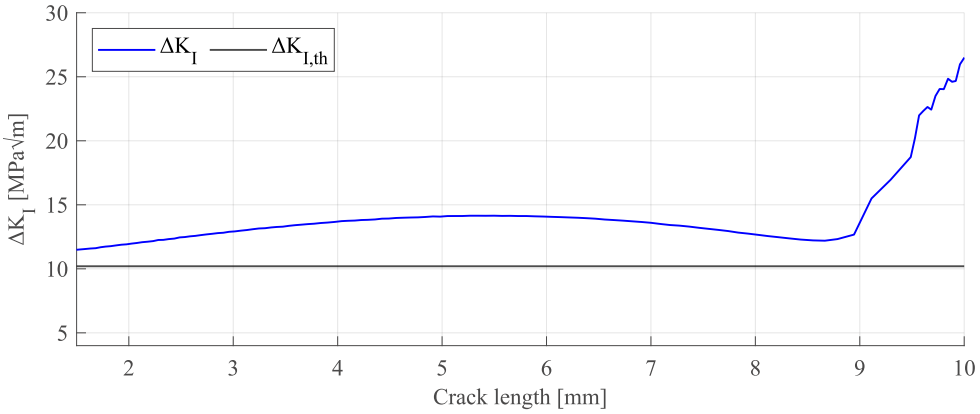

Figure 4.5. Simulated ΔK_I without considering FSI inside the crack shown for crack lengths of 1.5 to 10 mm.

5. RESULTS OF THE FSI APPROACH

The load profile under investigation (Figure 5.1) consists of the low-pressure level p_{min}, the pressure build-up dp_{bu}/dt , the high-pressure level p_{max} and the pressure drop dp_{dr}/dt.

The partitioning of the load cycle ensures that the individual load components are clearly separated and can therefore be investigated in a targeted manner. Furthermore, the interactions of pressure levels, holding times and pressure gradients can be examined. The low-pressure duration t_{LP} includes the period at low pressure and the pressure build-up, while the high-pressure duration t_{HP} includes the period at high pressure and the pressure drop. From these durations, a frequency f can be derived to further describe the cyclic load:

$$f = \frac{1}{t_{LP} + t_{HP}} \qquad (5.1)$$

Additionally, a high-to-low-pressure-duration ratio R_t is introduced:

$$R_t = \frac{t_{HP}}{t_{LP}} \qquad (5.2)$$

The load profile was also used in Michiels [4] and is inspired by pressure impulse tests, e.g. described in EN ISO 6803:2017.

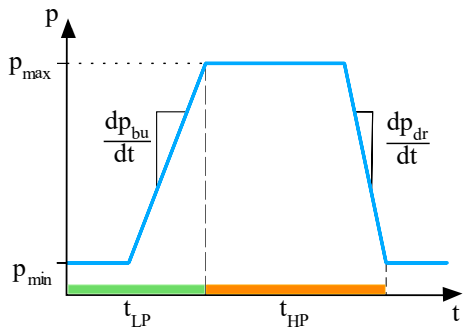

Figure 5.1. Schematic pressure load profile of the test specimen with the duration

The pressure build-up gradient was varied at three levels: 5, 12.5 and 20 kbar/s. The pressure drop gradient was varied at 5, 25 and 45 kbar/s. As this study focuses on pressure gradients, the maximum and minimum pressures were kept constant at p_{max} = 400 bar and p_{min} = 40 bar, respectively. The high-to-low pressure duration ratio was set to R_t = 1 and the excitation frequency to 6 Hz. The FSI simulations were performed for six discrete crack lengths a ∈ {1.5, 3, 4.5, 6, 7.5, 9} mm. Figure 5.2 shows the pressure profile over two load pulses within a crack of length a = 4.5 mm at different positions, for a pressure drop gradient of dp_{dr}/dt = 45 kbar/s and a pressure build-up gradient of dp_{bu}/dt = 12.5 kbar/s.

During pressure build-up, the pressure inside the crack increases with a noticeable delay compared to the system pressure in the pressure chamber. This delay is greater at positions deeper inside the crack. The duration of the investigated high-pressure phase is sufficient to approach the system pressure in the entire crack volume. After the system pressure drops, pressure peaks occur at various positions along the crack. This behaviour suggests that fluid is being entrapped during crack closure, leading to localized pressure increases. The highest pressure of 1440 bar is observed at the crack tip. In contrast, close to the crack mouth at x = 0.25 mm, the pressure decreased without returning to the initial low-pressure level p_{min}. The pressure at the crack mouth equals the system pressure during the whole load cycle due to the set boundary condition.

As the system pressure remains at a low-pressure level following the pressure drop, fluid can gradually escape the crack, resulting in decreasing pressure. A renewed pressure increase in the pressure chamber initially causes a pressure release at the observed positions. Close to the crack mouth (at x = 0.25 mm), the pressure drops shortly before increasing to the system pressure again. Deeper inside the crack the pressure drops to 0 bar and remains at this pressure level for a short period. While a low pressure inside the crack can be explained by the rapid opening of the crack in response to the pressure increase in the pressure chamber, the recorded value of 0 bar is still unrealistically low. This discrepancy is likely caused by insufficient volume flow in the model. Pressure close to the crack mouth does not drop to 0 bar, because of the resupply from the pressure chamber. The 0 bar pressure level is again followed by a subsequent increase to the system pressure that is delayed the deeper inside the crack. The high pressure duration is long enough to allow pressure equalization to p_{max} throughout the crack. In comparison to the former specimen with a shorter ligament of 5 mm, [4], the current simulated pressure profiles follow an equal pattern for a similar crack length.

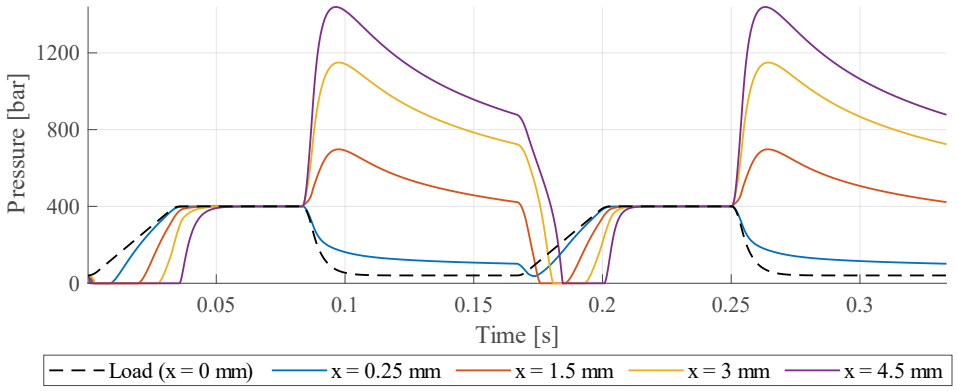

Figure 5.2. Pressure profile along the crack length a = 4.5 mm at various positions over time. The coordinate x = 0 mm corresponds to the crack mouth connected to the pressure chamber, while x = 4.5 mm represents the crack tip. The pressure distribution results from a load applied in two successive pulses.

Figure 5.2 displays the Mode I SIFs together with the corresponding system pressure over time for a crack length of 4.5 mm and the described load configuration. To evaluate the influence of the FSI, the SIF was calculated both with and without considering the fluid in the crack. The FSI accounts for hydrostatic pressure acting on the crack faces as well as fluid-induced crack closure effects. Without FSI, the SIF shows a strong correlation with the system pressure and the SIF range ΔK_I spans a wide interval. When fluid effects are considered $\Delta K_{I,eff}$ is reduced, indicating a lower crack propagation rate according to Paris' law (equation 2.4). Although higher peak values of the SIF are observed, the SIF does not drop significantly, presumably due to crack closure mechanisms. Overall, the comparison of SIF with and without FSI is in good agreement with the theoretical predictions of chapter 2, confirming that the influence of fluid on crack propagation is captured by the model.

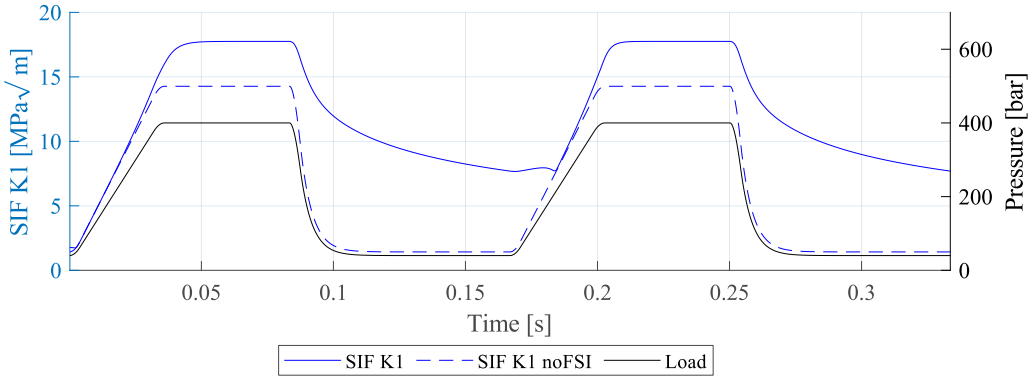

Figure 5.3. Comparison of the SIFs with and without considering the FSI (hydrostatic pressure on crack faces and fluid-induced crack closure). Left axis displays the mode I SIF, the right axis the corresponding system pressure.

According to Paris' law and the above-mentioned material parameters, this load case leads to a crack propagation rate of 0.729 µm per 1000 cycles for the evaluated crack length and load configuration, considering the FSI. Without the hydrostatic pressure and crack closure effects a crack growth rate of 1.5 µm per 1000 cycles was calculated, indicating a faster crack propagation due to a higher effective SIF range $\Delta K_{I,eff}$ at the crack tip for cracks without FSI. Figure 5.4 compares the mean crack propagation rate as a function of pressure drop rate and pressure build-up rate for cases with and without FSI effects averaged over the crack lengths. Crack propagation increases slightly as the pressure drop rate rises, with even higher growth rates predicted when FSI is neglected. In contrast, the influence of pressure build-up rate is comparatively weak, with only minor variations in crack propagation observed.

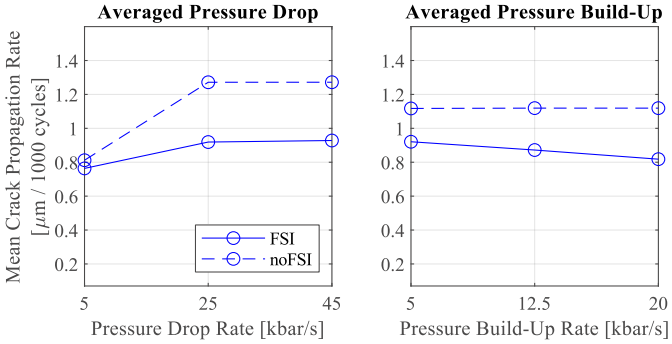

Figure 5.4. Comparison of the average crack propagation rate with and without FSI as a function of pressure drop rate and pressure rise rate. The values shown are averaged over the crack lengths (main effects).

Figure 5.5 shows the crack propagation rates of the discretely simulated crack lengths as a function of the pressure drop and build-up rates. These values primarily serve as a reference for comparison in future investigations. A clear trend can be observed indicating that the

crack propagation rate increases with increasing crack length, corresponding with the introduced crack propagation law by Paris (equation 2.4).

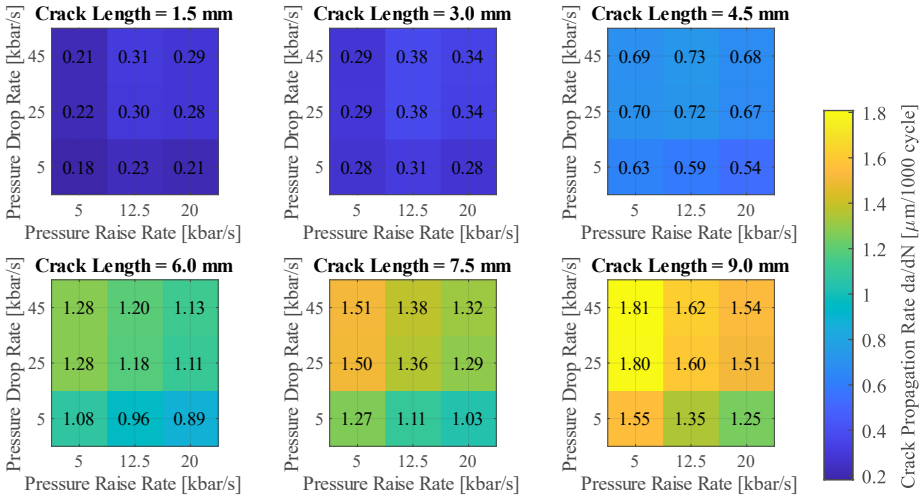

Figure 5.5. Crack propagation rates of discretely simulated crack lengths as a function of pressure drop and build-up rates and considering FSI effects.

6. Discussion and Outlook

In this work, a new version of the test specimen was developed according to extended and refined requirements to enable reproducible crack initiation, longer measurable crack propagation, and efficient manufacturability for a larger test campaign. Simulations showed that the test specimen experiences stable crack propagation without FSI under cyclic loading. The new specimen was implemented into the existing FSI framework. A plausible pressure profile for the first pressurization is achieved. However, during the second pressurization an unexpected depressurization down to 0 bar is observed, motivating a refinement of the simulation in the future. Furthermore, crack propagation rates for all configurations of pressure build-up and drop rate have been simulated. Within the considered interval, an increase in pressure drop rate shows a small influence on fatigue, resulting in a slightly shorter lifetime, while the build-up rate does not have a significant effect. The calculated values serve primarily as a reference point for future improvements.

In future work, the fluid domain should be extended to account for the crack width in a two-dimensional formulation. Fluid flow within the crack is expected to occur not only in the primary x-direction, but also in multiple directions within the crack plane. Introducing an additional spatial dimension would require the definition of an associated flow factor for this direction. As flow factors are defined along main roughness directions [17], this introduces a strong directional dependence of the surface roughness representation and consequently, of the volume flow. For non-isotropic roughness, this assumption is only valid if defined main roughness directions exist and agree with the directions for which the flow factors are defined. Otherwise, the resulting flow description becomes inaccurate. Alternatively, a different approach for modelling surface roughness should be employed. In [24], Rom et al.

compared the average flow model proposed by Patir and Cheng with a homogenization-based approach using a journal and slider bearing. They showed that the homogenization approach provides higher accuracy in predicting averaged pressure distributions while maintaining a comparable computational cost. Furthermore, the homogenization method can account for surface roughness of arbitrary anisotropy. In contrast to the flow factor approach, it offers greater flexibility when applied to non-isotropic surfaces.

Further limitations arise from the simplified fluid modelling assumptions. In particular, the assumptions of laminar, fully developed flow are insufficient to adequately represent the strongly transient flow conditions occurring within propagating cracks. In addition, possible cavitation effects resulting from the low pressure levels observed inside the crack after the pressure drop should be investigated.

Pulsation experiments will be used to compare and calibrate the current approach and following improvements. Furthermore, while the microholes have been considered in the calculation of the weight functions, their influence on the fluid flow, whose influence on fluid flow has not yet been considered will be addressed.

ACKNOWLEDGEMENTS

This work was funded by the German Research Foundation (DFG) in the scope of the project „Einfluss der Belastungsgradienten auf das Ermüdungsverhalten hydraulischer Komponenten" with the number 449676223. The authors would like to thank DFG for its support.

7. REFERENCES

[1] L. Brinkschulte, 'Assistenzsysteme zur Reduktion des Schädigungsverhaltens von Komponenten einer mobilen Arbeitsmaschine', Karlsruher Institut für Technologie, Karlsruhe, 2021. doi: 10.5445/KSP/1000130176.

[2] F. H. Davis and E. G. Ellison, 'Hydrodynamic Pressure Effects of Viscous Fluid Flow in a Fatigue Crack', Fatigue Fract. Eng. Mater. Struct., vol. 12, no. 6, pp. 527–542, Nov. 1989, doi: 10.1111/j.1460-2695.1989.tb00561.x.

[3] F. H. Davis, E. G. Ellison, and W. J. Plumbridge, 'Effects of Hydrostatic Pressure on the Rate of Fatigue Crack Growth', Fatigue Fract. Eng. Mater. Struct., vol. 12, no. 6, pp. 511–525, Nov. 1989, doi: 10.1111/j.1460-2695.1989.tb00560.x.

[4] L. Michiels, 'A simulation-based approach to the fluid-structure interaction inside fatigue cracks in hydraulic components', Karlsruher Institut für Technologie, Karlsruhe, 2024. Accessed: Feb. 06, 2025. [Online]. Available: https://publikationen.bibliothek.kit.edu/1000171515

[5] D. Gross and T. Seelig, Bruchmechanik. Berlin, Heidelberg: Springer Berlin Heidelberg, 2016. doi: 10.1007/978-3-662-46737-4.

[6] M. Kuna, Finite Elemente in der Bruchmechanik: Theorie – Numerik – Anwendungen. Wiesbaden: Springer Fachmedien Wiesbaden, 2025. doi: 10.1007/978-3-658-46192-8.

[7] P. Paris and F. Erdogan, 'A Critical Analysis of Crack Propagation Laws', J. Basic Eng., vol. 85, no. 4, pp. 528–533, Dec. 1963, doi: 10.1115/1.3656900.

[8] W. Elber, 'Fatigue crack closure under cyclic tension', Eng. Fract. Mech., vol. 2, no. 1, pp. 37–45, Jul. 1970, doi: 10.1016/0013-7944(70)90028-7.

[9] H. A. Richard and M. Sander, Fatigue Crack Growth, vol. 227. in Solid Mechanics and Its Applications, vol. 227. Cham: Springer International Publishing, 2016. doi: 10.1007/978-3-319-32534-7.

[10] S. Ismonov and S. R. Daniewicz, 'Simulation and comparison of several crack closure assessment methodologies using three-dimensional finite element analysis', Int. J. Fatigue, vol. 32, no. 8, pp. 1322–1329, Aug. 2010, doi: 10.1016/j.ijfatigue.2010.01.016.

[11] E08 Committee, Test Method for Measurement of Fatigue Crack Growth Rates. doi: 10.1520/E0647-24.

[12] F. H. Davis and E. G. Ellison, 'Hydrodynamic Pressure Effects of viscous Fluid Flow inside a fatigue crack', Fatigue Fract. Eng. Mater. Struct., vol. 12, no. 6, pp. 527–542, Nov. 1989, doi: 10.1111/j.1460-2695.1989.tb00561.x.

[13] M. Akama and T. Mori, 'Boundary Element Analysis of Effects of Crack Face Friction and Trapped Fluid on Rolling Contact Fatigue Cracks', Q. Rep. RTRI, vol. 46, no. 4, pp. 231–237, 2005, doi: 10.2219/rtriqr.46.231.

[14] D. I. Fletcher, P. Hyde, and A. Kapoor, 'Investigating fluid penetration of rolling contact fatigue cracks in rails using a newly developed full-scale test facility', Proc. Inst. Mech. Eng. Part F J. Rail Rapid Transit, vol. 221, no. 1, pp. 35–44, Jan. 2007, doi: 10.1243/09544097JRRT63.

[15] A. F. Bower, 'The Influence of Crack Face Friction and Trapped Fluid on Surface Initiated Rolling Contact Fatigue Cracks', J. Tribol., vol. 110, no. 4, pp. 704–711, Oct. 1988, doi: 10.1115/1.3261717.

[16] N. Patir and H. S. Cheng, 'An Average Flow Model for Determining Effects of Three-Dimensional Roughness on Partial Hydrodynamic Lubrication', J. Lubr. Technol., vol. 100, no. 1, pp. 12–17, Jan. 1978, doi: 10.1115/1.3453103.

[17] N. Patir and H. S. Cheng, 'Application of Average Flow Model to Lubrication Between Rough Sliding Surfaces', J. Lubr. Technol., vol. 101, no. 2, pp. 220–229, Apr. 1979, doi: 10.1115/1.3453329.

[18] G.-J. Deng, S.-T. Tu, X.-C. Zhang, Q.-Q. Wang, and C.-H. Qin, 'Grain size effect on the small fatigue crack initiation and growth mechanisms of nickel-based superalloy GH4169', Eng. Fract. Mech., vol. 134, pp. 433–450, Jan. 2015, doi: 10.1016/j.engfracmech.2015.01.002.

[19] D. L. McDowell and F. P. E. Dunne, 'Microstructure-sensitive computational modeling of fatigue crack formation', Int. J. Fatigue, vol. 32, no. 9, pp. 1521–1542, Sep. 2010, doi: 10.1016/j.ijfatigue.2010.01.003.

[20] K. Kida, T. Yamazaki, M. Shibata, N. Oguma, and H. Harada, 'Crack initiation from micro surface holes in bearings under rolling contact fatigue', Fatigue Fract. Eng. Mater. Struct., vol. 27, no. 6, pp. 481–493, Jun. 2004, doi: 10.1111/j.1460-2695.2004.00771.x.

[21] Y. Murakami and M. Endo, 'Effects of defects, inclusions and inhomogeneities on fatigue strength', Int. J. Fatigue, vol. 16, no. 3, pp. 163–182, Apr. 1994, doi: 10.1016/0142-1123(94)90001-9.

[22] ANSYS Mechanical. ANSYS, Inc., Canonsburg, Pennsylvania, USA. [Online]. Available: https://www.ansys.com/

[23] T. L. Anderson, Fracture mechanics: fundamentals and applications, 2nd ed. Boca Raton Ann Arbor London [etc.]: CRC press, 1995.

[24] M. Rom, F. König, S. Müller, and G. Jacobs, 'Why homogenization should be the averaging method of choice in hydrodynamic lubrication', Appl. Eng. Sci., vol. 7, p. 100055, Sep. 2021, doi: 10.1016/j.apples.2021.100055.

Biographies

Fabian Blatter studied mechanical engineering at the Karlsruhe Institute of Technology. He is currently working as a Research Associate at the Department of Mobile Machines at the Karlsruhe Institute of Technology. His research areas include simulation of fluid-structure-interaction and hydraulic applications.

Lukas Boden obtained his master's degree in mechanical engineering at RWTH Aachen University in 2023. Since then, he is working as a research assistant at the Institute for Fluid Power Drives and Systems (ifas), focussing on identifying the influence of viscous fluid on fatigue crack propagation in fluid power components.

Prof. Dr.-Ing. Marcus Geimer received the Diploma degree in mechanical engineering from the RWTH Aachen University, Germany, in 1990, and the Ph.D. degree from the Institute of Hydraulics and Pneumatics, today named the Institute for Fluid Power Drives and Systems, RWTH Aachen University. Since 2005, he has been a Full Professor and the Director of the Institute of Mobile Machines (Mobima), Karlsruhe Institute of Technology (KIT), Germany. He started his industrial career in 1995 in the field of construction at the company Krupp Berco Bautechnik GmbH, Germany, where he was the Leader of the research group for hydraulic breakers. In 2000, he was with Bucher Hydraulics GmbH, Germany, where he led the construction and customer development for mobile hydraulics.

Prof. Dr.-Ing. Katharina Schmitz studied mechanical and chemical engineering at RWTH Aachen University and Carnegie Mellon University, Pittsburgh (USA) and graduated 2015 as Dr.-Ing. at RWTH Aachen University. Since 2018, she is full professor at RWTH Aachen University and director of the Institute for Fluid Power Drives and Systems (ifas). In addition, she is Vice Dean of the Faculty for Mechanical Engineering at RWTH Aachen, a position she holds since 2020. Prof. Schmitz's awards and honors include several best paper awards and 2023 IMechE Joseph Bramah Medal award.